JOURNAL OF AIRCRAFT
Vol. 39, No. 1, January–February 2002

Some Factors of Hypersonic Inlet/Airplane Interactions

Y. P. Goonko* and I. I. Mazhul†
Russian Academy of Sciences, Novosibirsk, 630090, Russia

Results of an experimental study are presented on aerodynamics of a hypersonic vehicle whose air-breathing engine nacelle, including a two-dimensional inlet, is located under the lifting body. Experiments with a ducted model were performed in a blow-down wind tunnel at $M_\infty = 4$ and 6. Aerodynamic forces acting on the model were measured with a balance; aerometry of the inlet-captured airstream was carried out; parameters of the boundary layer in front of the inlet were also measured. Problems of inlet/airplane interaction such as wedge-aided diversion of the boundary layer developed upstream of the inlet, lateral flow spillage over the wedge ramp of the inlet with and without side cheeks, and forebody nose bluntness were studied. Effects of these factors on the inlet flow-rate, the total aerodynamic and performance characteristics of the vehicle as a whole were revealed. The resultant aeropropulsive characteristics, which showed flight properties of the vehicle, were obtained by combining experimental aerodynamic data and calculated estimates of the thrust of the engine in a scramjet mode. Aeropropulsive force polars demonstrated some special path instability of the vehicle and an extraordinary behavior of these polars in the case of the blunted forebody.

Nomenclature

A = cross-sectional area, m^2
A_0 = frontal area of the inlet, m^2
A_∞ = cross-sectional area of the free airstream captured by the inlet, m^2
$\bar{A}_{\text{ch}}$ = relative cross-sectional area of the plenum chamber in the model duct, $A_{\text{ch}}/A_{\text{th}}$
$\bar{A}_{\text{en}}$ = relative cross-sectional entrance area of the inlet, A_{en}/A_0
$\bar{A}_{\text{nz}}$ = relative cross-sectional area of the metering nozzles at the duct exit, $\sum_{1}^{N_{\text{nz}}} \frac{A_{\text{nz}}}{A_{\text{th}}}$
$\bar{A}_{\text{th}}$ = relative cross-sectional throat area of the inlet, A_{th}/A_0
$\bar{A}_0$ = relative frontal area of the inlet, A_0/S_{pl}
A^* = cross-sectional area covered by boundary-layer displacement thickness δ^*, m^2
b, h = width and height of a component of the aerodynamic configuration, mm
C_D = aerodynamic drag coefficient, $D/q_\infty S_{\text{pl}}$
C_{D_0} = drag coefficient at $C_L = 0$
C_L = aerodynamic lift coefficient, $L/q_\infty S_{\text{pl}}$
C_L^α = C_L derivative with respect to the angle of attack, deg^{-1}
C_{R_x} = coefficient of resultant aeropropulsive tangential force, $R_x/q_\infty S_{\text{pl}}$,
C_{R_y} = coefficient of resultant aeropropulsive lift force, $R_y/q_\infty S_{\text{pl}}$
C_T = engine thrust coefficient, $T/q_\infty A_0$
D = aerodynamic drag force or x-component of the resultant aerodynamic force, $-\boldsymbol{R}_{a_x}$
d_{nz} = diameter of the metering nozzle, mm
f = flow-rate factor of the inlet, A_∞/A_0
H_{bl} = boundary-layer shape factor, δ^*/δ^{**}
H_u = fuel calorific value, J/kg
h_{blw} = height of wedges for boundary-layer diversion (diversion wedges), mm
I = total momentum of the flowstream, N; for the one-dimensional flowstream, $mV + (p - p_\infty)A$
L = aerodynamic lift force or y-component of the resultant aerodynamic force, $\boldsymbol{R}_{a_y}$
L_{tr} = length of boundary-layer transition, mm
L/D, $(L/D)_{\max}$ = lift-to-drag ratio, maximal lift-to-drag ratio
L_0 = stoichiometric mass air-to-fuel ratio
l = span of the lifting configuration, m
M = flow Mach number
M_d = inlet design Mach number
M_∞ = freestream Mach number
m = mass flow rate, kg/m^{2}s; for the one-dimensional flowstream, ρVA
N_{nz} = number of metering nozzles
$\boldsymbol{n}$ = unit-directing vector
p = pressure, N/m^2
q_∞ = freestream dynamic pressure, N/m^2
$\boldsymbol{R}$ = vector of the resultant aeropropulsive force
$\boldsymbol{R}_a$, R_{a_x}, R_{a_y} = vector of the resultant aerodynamic force and its x and y components
R_{air}, R_f, R_{cp} = specific constants for air, fuel, and combustion products, respectively
R_b = radius of bluntness of the lifting-body nose or the leading edge of the inlet, mm
R_g = specific gas constant, J/kg/K
R_x = tangential component (x component) of the resultant aeropropulsive force
R_y = lift component (y component) of the resultant aeropropulsive force
$Re_{1\infty}$ = freestream Reynolds number per meter, 1/m
Re_{tr} = Reynolds number of boundary-layer transition
Rz = roughness parameter, μm
S = plan area of the lifting configuration or wing, m^2
S_{pl} = reference plan area of the model configuration, m^2
$\boldsymbol{T}$ = vector of engine thrust
t = temperature, K
V = velocity, m/s
x, y, z = aerodynamic coordinate axes accepted in Russia, see Fig. 1
α = angle of attack, deg

Received 12 February 2001; revision received 5 September 2001; accepted for publication 26 September 2001.

*Head of Research Group, Institute of Theoretical and Applied Mechanics, Siberian Branch. Experimental Aerodynamics Laboratory.
†Senior Research Scientist, Institute of Theoretical and Applied Mechanics, Siberian Branch. Experimental Aerodynamics Laboratory.

α_{af} = air-to-fuel ratio
γ = adiabatic exponent (or specific heat ratio)
δ, δ^*, δ^{**} = boundary-layer thickness, displacement thickness, and momentum thickness, mm
θ = wedge angle, deg
θ_1, θ_2, θ_2 = wedge angles of the triple-shock inlet ramp, deg
λ = aspect ratio of the lifting configuration, l^2/S_{pl}
ρ = density, kg/m^3
σ = total-pressure recovery factor
χ = sweep angle, deg

Subscripts

a = aerodynamic forces
b = bluntness
bal = balance-measured forces
base = base face of the body
bl = boundary layer
blw = wedge for boundary-layer diversion
ch = plenum chamber of the model duct; engine combustion chamber
cp = combustion products
duct = model duct forces
en = entrance of the internal duct of the inlet
eng = airbreathing engine
ext = forces over external surfaces of the airplane including the engine nacelle
fuel = fuel parameters
inl = inlet parameters
int = internal section of the inlet from the entrance to the throat
lb = lifting body
m = midsection
nz = metering nozzle of the model duct
nze = engine nozzle
ss = forces over surface of the inlet-captured airstream
supp = support of the model
sw = shock wave parameters
th = inlet throat
w = wing, also wall
0 = total (stagnation) flow parameters
∞ = freestream parameters

Introduction

A DISTINCTIVE feature of hypersonic vehicles powered by airbreathing engines is a high degree of interaction and integration of the propulsion unit and the airplane. Problems of this kind are typical, in particular, of configurations with the engine nacelle located under the lifting body or the wing, which are conventional for hypersonic scramjet-powered vehicles. One of these problems is associated with the lifting surfaces of the vehicle forebody or the wing simultaneously acting as precompression surfaces of the airstream captured by the inlet. The boundary layer developing on such a surface and entering the inlet may have an adverse effect on the inlet and engine performance. The latter may be improved by placing the inlet outside the boundary layer, for example, by installing it on wedges for boundary-layer diversion. Obviously, these wedges will increase somewhat the drag of the vehicle. Thus, the efficiency of such boundary-layer diversion will be determined by the compromise between the improvement of the internal characteristics of the inlet and engine and the increase in the external drag of the vehicle. Therefore, investigations of this kind of wedge-aided diversion of the boundary layer should include an integrated analysis of its effects not only on the characteristics of the inlet itself but also on the overall aerodynamic and aeropropulsive efficiency of the vehicle.

Presently, particular questions are generally considered that are related to the effects of the boundary layer and its diversion at high supersonic velocities on the characteristics of the inlets themselves, outside of their combining with an airplane. Some results of an experimental study (within the range $M_\infty = 2$–5) of these effects for a two-dimensional (flat) inlet mounted under a delta wing are presented in Refs. 1 and 2. It is shown that the adverse effect of the boundary layer developing on the wing surface is almost eliminated by shifting the inlet from the wing to a relative height $h/\delta = 0.5$–0.6, where δ is the boundary-layer thickness ahead of the inlet. In this case, the flow-rate and the pressure recovery factors of the inlet are 75–95% of those values that can be reached with complete diversion of the boundary layer. Measurements of the boundary layer developing on forebody precompression surfaces upstream of an inlet, for hypersonic vehicles of various configurations, were performed in Ref. 3 for $M_\infty = 4$ and in Refs. 4 and 5 for $M_\infty = 6$. It was found[4,5] that the boundary-layer thickness in the plane of symmetry could reach 20–100% of the height of the inlet entrance cross section, depending on the vehicle configuration. The state and characteristics of the boundary layer developing on the compression wedge ramp of flat inlets mounted on diverter wedges was experimentally studied in Ref. 1 for $M_\infty = 2$–5 and in Ref. 3 for $M_\infty = 2$–4. The flow around various such wedges with dummy boxlike inlets mounted on them and the drag of these wedges were studied in Refs. 6 and 7 for supersonic velocities ($M_\infty = 1.0$–2.5). In particular, it was shown[7] that, for $M_\infty = 2.25$, diverter wedges with a swept leading edge of $\chi_{blw} \geq 46$ deg have a lower drag (by 15–20%) as compared to the wedge variant with $\chi_{blw} = 0$.

There is almost no literature dealing with effects of wedge-aided diversion of the boundary layer on the total aerodynamic and aeropropulsive characteristics of scramjet-powered hypersonic vehicles as a whole. Only Refs. 8 and 9 are recalled. In Ref. 8, estimates of the resultant aeropropulsive characteristics of a scramjet-powered vehicle were obtained using approximate calculation methods. It was shown that boundary-layer diversion with the use of wedges may improve the resultant characteristics of the vehicle within the freestream Mach number range from $M_\infty \approx 4$ to $M_\infty = 7$–10. Note that the efficiency of wedge-aided diversion of the boundary layer decreases with increasing M_∞. Goonko et al.[9] give some experimental support to the integral approach proposed in Ref. 8 for evaluation of the effect of boundary-layer diversion ensured by wedges on the performance of a hypersonic scramjet-powered vehicle as a whole. The vehicle configuration considered here was studied in Ref. 9, and the main results obtained are outlined in the present paper in association with other factors of hypersonic inlet/airplane interaction investigated by the authors more recently.

In studying the characteristics and preliminary designing of scramjet-powered hypersonic vehicles, two-dimensional or quasi-two-dimensional supersonic inlets with a multiwedge compression ramp are widely spread. For two-dimensional inlets, the design regime is usually identified with $M_\infty = M_d$ for which the plane oblique shock waves forming on the ramp wedges are focusing on the leading edge of the inlet cowl lip. Such a design flow regime for a flat inlet really may be achieved if the shock wave forming on the first wedge of the ramp is aligned with the plane of the swept leading edges of the side cheeks restricting the design flow region in the lateral directions. In off-design regimes for the inlets designed in such a manner, for instance, at Mach numbers $M_\infty < M_d$, the shocks come out above these leading edges of the cheeks, and the flow over the compression ramp is no longer strictly two dimensional because of lateral flow spillage. Similar lateral spillage also arises if the cheeks restrict the compression flow region near the ramp only partly (short cheeks) or if there are no cheeks.

The effects of three dimensionality of the flow around a multiwedge compression ramp on the characteristics of flat inlets, with cheeks of various shapes and without them, were studied, for example, in Refs. 2 and 10–12. It was noted[2] that, for flat inlets with the width-to-height ratio $b_{inl}/h_{inl} \geq 4$, the lateral spillage over the compression ramp weakly affects the flow-rate factor depending on the configuration of the cheeks. At the same time, the numerical computations[10,11] show that, in flow around the inlet with short side cheeks, internal shock waves form on the latter because of slip deflection of the flow near the compression ramp. Investigations have not as yet been carried out of possible effects of lateral flow spillage near the compression ramp on the characteristics of the flat inlets combined with the airplane and on the characteristics of the vehicle as a whole.

The flight of vehicles at high hypersonic speeds is accompanied by intense aerodynamic heating. Therefore, the nose tips and the leading edges of the forebody and other elements of these vehicles should be blunted. The bluntness dimensions are usually small relative to the vehicle dimensions, but strong normal-curved shock waves form over a blunted nose or leading edge. The inlet flow structure can significantly change the overall pattern of the external flow around the vehicle, especially for vehicles powered by airbreathing engines, as compared to equivalent pointed bodies. A high-entropy layer can form near the surface of such a blunted body, which is characterized by high nonuniformity and low Reynolds numbers for the layer flow. Under these conditions, the development of the boundary layer, its integral characteristics, and its effect on the inlet performance may also significantly differ from those for a sharp configuration.

The effects of blunted leading edges of the compression wedge ramp, side cheeks, and cowl lip on the performance of a flat inlet was experimentally studied for $M_\infty = 4$–5.5 in Ref. 13. It is shown that the small bluntness of the cowl lip and side cheeks has a weak effect on the flow-rate factor of the inlet. In contrast to that, the bluntness of the leading edge of the ramp wedge has a significant effect. For a rather large bluntness (with a radius $R_b \approx 0.025\, h_{\text{inl}}$), the operating regime of a started inlet may be destroyed. The shape of leading-edge bluntness of the ramp wedge also exerts a significant effect. The effect of blunted leading edges of a delta wing on the characteristics of an inlet mounted under this wing was studied experimentally in Ref. 13 and numerically, for an inviscid flow, in Ref. 14. An increase in the wing bluntness radius is accompanied by a decrease in the inlet flow-rate factor[13,14] and can also lead to flow stalling ahead of the inlet entrance.[13] The adverse effect of wing bluntness decreases[13] with increasing angle of attack and sweep angle of the wing or with moving the inlet away from the wing surface, that is, in the case where the boundary layer is diverted partially or completely. An analysis of the drag produced by the blunted leading edges themselves as applied to supersonic and hypersonic inlets can be found in Ref. 15. The effects of nose bluntness of the forebody on the characteristics of the inlet, engine, and vehicle as a whole have not been adequately studied yet; this is particularly true for the total aeropropulsive characteristics.

The objective of the presented work was an experimental study of the influence of the mentioned factors of inlet/airplane interaction (boundary-layer diversion, lateral flow spillage over the compression wedge ramp of the inlet, and nose bluntness of the forebody) on the characteristics of scramjet-powered hypersonic vehicles. In contrast to many cited papers dealing with particular aspects, an attempt was made to perform an integrated analysis of these factors extending the works.[8,9] We consider their effects, first, on the characteristics of the inlet itself, taking into account its integration with the lifting body and, second, on the total aerodynamic and aeropropulsive characteristics of the vehicle as a whole.

Model and Test Conditions

The experimental study was performed with a schematized model representing a scramjet-powered vehicle, which consists of a lifting body (fuselage), a delta wing, and a scramjet engine nacelle located in a ventral position under the lower surface of the body (Fig. 1). The body and the wing form a total lifting delta configuration with leading edges of sweep $\chi = 80$ deg. The lifting body has a trapezoidal cross section of its forebody transformed to a rectangular one at the tail of its rearbody. A lower triangular plane surface of the forebody is a precompression surface of an airstream captured by the inlet. The wing has a lower plane surface and a wedge-shaped airfoil of angle $\theta_w = 3$ deg. The overall dimensions (in millimeters) of the model are given in Fig. 1. The model configuration considered is characterized by the following parameters: reference plan area of the model $S_{\text{pl}} = 0.0936$ m^2, aspect ratio of the overall lifting planform surface $\lambda = 0.708$, relative planform area of the wing $S_w/S_{\text{pl}} = 0.305$, relative area of the base cross section of the lifting body together with the engine nacelle $A_{\text{lb}}/S_{\text{pl}} = 0.084$, and relative area of the midsection of the airplane including the wing and the engine nacelle $A_m/S_{\text{pl}} = 0.09$. The body has a replaceable nose tip, which can be pointed or three dimensionally blunted; the bluntness radii are $R_b = 7$ mm in the plan view ($2R_b/b_{\text{lb}} = 0.122$, where $b_{\text{lb}} = 115$ mm is the lifting body width) and $R_b = 2.5$ mm in the vertical plane of symmetry ($2R_b/h_{\text{lb}} = 0.124$, where $h_{\text{lb}} = 40$ mm is the lifting body height).

The overall dimensions of the model are made with tolerances no more than -0.7 mm. The inlet tolerances are -0.1 mm in length, -0.07 mm in width, and ± 0.03 mm in throat height; deviations of the ramp wedges are no more than ± 17 minute of an arc. The roughness of external aerodynamic surfaces of the model and compression surfaces of the inlet is not worse than $Rz = 20\ \mu$m and, apparently, $Rz = 2.5\ \mu$m.

The general arrangement of the engine nacelle and the model duct is shown in Fig. 2. The inlet has a triple-shock wedge ramp of external compression with wedge angles $\theta_1 = 7.5$, $\theta_2 = 15$, and $\theta_3 = 22.5$ deg. For a design Mach number $M_d = 6$, which refers to the inlet proper, plane shock waves arising on the ramp wedges should intersect on the leading edge of the inlet cowl. The inlet cowl is made without bending its lip. The frontal area of the inlet is $A_0 = b_{\text{inl}} h_{\text{inl}}$, where $b_{\text{inl}}/h_{\text{inl}} \approx 1.91$ and $b_{\text{inl}} = 68.3$ mm and $h_{\text{inl}} = 35.6$ mm are the height and width of the inlet by its leading edges including those of the wedge ramp, the side cheeks, and the cowl. Its relative value is $\bar{A}_0 = 0.026$. The inlet has the simplest geometry of the input section of the internal duct with a relative entrance area and throat area $\bar{A}_{\text{en}} \approx \bar{A}_{\text{th}} \approx 0.2$. The inlet throat is rather short with a relative length of about twice its height and with a small flare of an angle about 2 deg, downstream of which there is a 17-deg diffuser. The general arrangement of the model duct is made by requirements for aerodynamic testing the ducted models representing vehicles powered by airbreathing engines. These requirements are presented

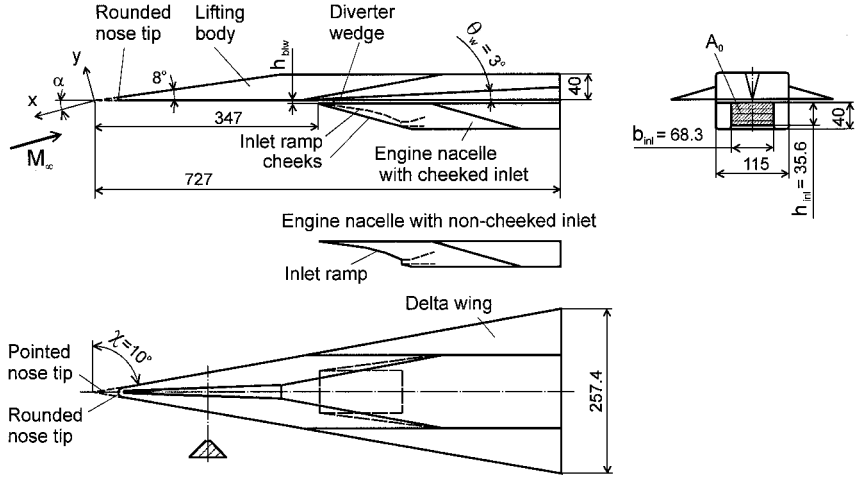

Fig. 1 General view of the tested model of a ramjet-powered vehicle.

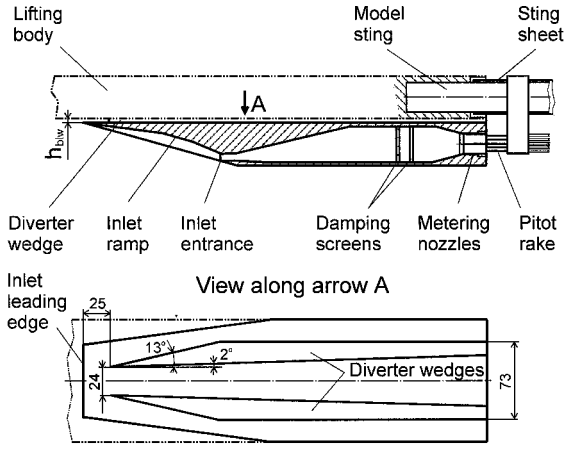

Fig. 2 General arrangement of the engine nacelle and the model duct.

in Ref. 16. Damping screens are mounted in the plenum chamber of the model duct with a relative area $\bar{A}_{ch} \approx 7.2$. Four narrow metering nozzles (plugs) are mounted at the model duct exit ($N_{nz} = 4$). Their diameter is chosen under the condition that the inlet should be started within the entire range of freestream parameters examined and that the rear normal shock arising in the internal duct flow should be located in the inlet diffuser. The experimental data presented were obtained for $d_{nz} = 15.6$ mm, and the total relative exit area of the metering nozzles is $\bar{A}_{nz} = 1.62$. A pitot rake for aerometry of flow parameters in the metering nozzles is installed at the nacelle duct exit (Fig. 2).

The model is equipped with two replaceable engine nacelles, which differs by the presence or absence of the side cheeks (walls) along the inlet wedge ramp, but the geometric parameters of the ducts and the main lines of the external contour were identical (Fig. 1). In tests with boundary-layer diversion, one or the other nacelle can be mounted on two symmetrically located diverter wedges of height h_{blw}. The geometry of these wedges is shown in Fig. 2. The wedges of height $h_{blw} = 2$ and 3.7 mm and $h_{blw} = 3$ and 5 mm were used in experiments for $M_\infty = 4$ and 6, respectively.

The model was tested in the supersonic blowdown wind tunnel T-313 (Ref. 17) based at Institute of Theoretical and Applied Mechanics (Novosibirsk, Russia). This wind tunnel has a rectangular test section of 0.6×0.6 m transverse dimensions and of 2.5 m length; interchangeable nozzle inserts provide flow Mach numbers in the range $M_\infty = 2$–6. It is equipped with a staff four-component mechanical-type balance, multichannel transducer for pressure measurement, and schlieren shadowgraph device. The instrumental error of balance measurement is less than 0.1% of the upper limit of the balance ranges. Respectively, in testing the model, the error of onefold measurement for the drag was 0.7–0.2% for $M_\infty = 4$ and 1.1–0.4% for $M_\infty = 6$; the error of lift force measurement was even smaller. The pressure transducer has the ranges of 0–10^5 N/m^2 and 0–6×10^5 N/m^2 with a measurement error of less than 0.3% of the upper limit of these ranges.

For the model considered, the test conditions included the following freestream parameters: $M_\infty = 4.05$, $Re_{1\infty} = 50 \times 10^6$ 1/m, and $q_\infty = 7.5 \times 10^4$ N/m^2 and $M_\infty = 6.06$, $Re_{1\infty} = 17.7 \times 10^6$ 1/m, and $q_\infty = 1.2 \times 10^4$ N/m^2. The stagnation temperature in the plenum chamber of the wind tunnel was $t_{0\infty} \approx 286$ K for the both Mach numbers.

The characteristics of the stream captured by the inlet and passing through the nacelle duct were measured at the duct exit using the metering nozzles and the pitot rake mentioned earlier. This aerometry was carried out simultaneously with the balance measurement; thus, the pitot rake did not affect the latter. These aerometric data were used to determine the flow-rate factor of the inlet and the forces over the internal surfaces of the duct. The latter were not simulated for a full-scale vehicle and were excluded from the resultant aerodynamic forces measured with the balance. Based on the data of Refs. 16 and 18, the total instrumental errors occurred in tests of ducted models in T-313 with the aerometric technique considered are as follows: the inlet flow-rate factor 1–4%, the drag at near-zero angles of attack about ~3.0% for $M_\infty = 4$ and ~8.7% for $M_\infty = 6$, and the maximal lift-to-drag ratio ~1.3% for $M_\infty = 4$ and ~3.8% for $M_\infty = 6$.

Note that the aerodynamic characteristics presented for the model considered include also the base drag over that part of the rear face of the lifting body and engine nacelle that is not occupied by the metering nozzles. There is some base drag of the wing, which also has a rear face because of a wedge-shaped profile. Estimates for the base drag of the airplane and engine nacelle yield ~6% for $M_\infty = 4$ and ~3% for $M_\infty = 6$.

All of the tests were performed with natural development of the boundary layer on the model surfaces. As evidenced by an analysis of velocity profiles in the boundary layer measured on the model configuration without nose bluntness for $M_\infty = 4$ and calculated estimates of the transition length for $M_\infty = 6$, the boundary layer immediately ahead of the inlet was turbulent.

Representation of Aerodynamic Forces of the Model

A technique for aerodynamic testing of ducted models of vehicles powered by airbreathing engines, which has been used before in Russia (see Ref. 16), was used for experimentation with the studied model. The essential feature of this technique is that the external flow around the vehicle and over the inlet is simulated, but the operation of the engine and the exhaust jet are not considered. Internal nonsimulated forces acting in the model duct are determined and excluded from the balance measurement results in this case; they are found from the change in the momentum of the inlet airstream captured by the inlet and passing through the duct. The flow-rate and momentum of this stream, which are required for this purpose, are determined by measuring flow parameters at the exit duct. Note, as this takes place, the flow-rate factor of the inlet integrated with the airplane is determined.

The flow rate m_∞ of the airstream captured by the inlet and passing through the model duct is determined from the mass flow continuity and by the flow rate measured at the duct exit using metering nozzles:

$$m_\infty = \sum_1^{N_{nz}} m_{nz}, \qquad m_{nz} = k_m \cdot q(M_{nz}) \cdot p_{0nz} \cdot \frac{A_{nz}}{\sqrt{t_{0nz}}} \tag{1}$$

Here

$$k_m = \sqrt{\gamma[2/(\gamma+1)]^{(\gamma+1)/(\gamma-1)}/R_g}$$

is a dimensional coefficient, K$^{1/2}$ s/m,

$$q(M) = M(2/(\gamma+1)\{1 + [(\gamma-1)/2]M^2\})^{-(\gamma+1)/2(\gamma-1)}$$

is a gasdynamic function of the reduced flow rate, $A_{nz} = \pi d_{nz}^2/4$, and M_{nz}, p_{0nz}, and t_{0nz} are the average values of the stream parameters in the metering nozzle. In testing the model under the freestream parameters considered, a critical choked flow occurred at the model duct exit, and the flow in a narrow metering nozzle was close to sonic. In accordance with this, the local total pressure in the nozzle can be taken equal to the pitot pressure measured. Note, in a general case of a supersonic flow, the total pressure behind the normal shock is measured with a pitot tube. The average total pressure p_{0nz} was determined by averaging over the area the pitot pressures measured with the rake in every nozzle. It was also assumed that $M_{nz} = 1$. The flow in the model duct was assumed to be adiabatic, and the thermophysical properties of air were assumed to be constant, that is, $t_{0nz} = \text{const} = t_{0\infty}$ and $\gamma = \text{const} = 1.4$.

The flow-rate factor of the inlet is found from the flow-rate equation (1) as

$$f = \frac{A_\infty}{A_0} = \frac{\sum_1^{N_{nz}} p_{0nz} \cdot q(M_{nz}) \cdot A_{nz}}{p_{0\infty} \cdot q(M_\infty) \cdot A_0} \tag{2}$$

The total aerodynamic forces obtained in testing a ducted model are determined in the form

$$\boldsymbol{R}_a = \boldsymbol{R}_{bal} - \boldsymbol{R}_{duct} - \boldsymbol{R}_{supp} \tag{3}$$

where $\boldsymbol{R}_a$ is the vector of the resultant aerodynamic force to be determined; $\boldsymbol{R}_{\text{bal}}$ is the vector of the resultant force acting on the model and measured by the balance; $\boldsymbol{R}_{\text{duct}}$ is the vector of the excluded resultant force of the duct, the components of $\boldsymbol{R}_{\text{duct}}$ are usually called duct-effect corrections; and $\boldsymbol{R}_{\text{supp}}$ is the vector of the force representing some methodical correction related to the manner of installing the model on a support of the aerodynamic balance. The last term was determined by a staff procedure accepted for the wind tunnel T-313 (Ref. 17) and is not considered here.

The forces acting in the model duct are found from the change in the momentum of the inlet-captured airstream with consideration of this stream portion between the cross section in the freestream flow to the duct-exit cross section. The excluded forces contain a part of duct forces that are not simulated for a full-scale vehicle and a part of modeled forces. Different forms of decomposition of these forces and, correspondingly, determination of internal nonsimulated forces are possible.[16] Hence, the aerodynamic characteristics of the same ducted model obtained in various ways may differ. In the presented work, we used the approach of Ref. 19 (discussed also in Ref. 16). According to Ref. 19, the forces involved by the deflection of the momentum vector of the inlet-captured airstream passing through the model duct refer to modeled forces and are not excluded. The forces arising as a result of the change in the magnitude of this momentum refer to nonsimulated forces and should be excluded from the balance measurement results. In accordance with Ref. 19, the duct-effect correction should be written as

$$\boldsymbol{R}_{\text{duct}} = -(I_{\text{nz}} - I_\infty)\cdot \boldsymbol{n}_{\text{nz}}$$

$$I_{\text{nz}} = \sum_{1}^{N_{\text{nz}}} [m_{\text{nz}} V_{\text{nz}} + (p_{\text{nz}} - p_\infty) A_{\text{nz}}]$$

$$= \sum_{1}^{N_{\text{nz}}} \left[p_{\text{nz}} \gamma M_{\text{nz}}^2 + (p_{\text{nz}} - p_\infty) A_{\text{nz}} \right]$$

$$I_\infty = m_\infty V_\infty = p_\infty \gamma M_\infty^2 f A_0 \tag{4}$$

where $\boldsymbol{n}_{\text{nz}}$ is the unit-directing vector of the axis of the metering nozzles, which is assumed to coincide with the vector $\boldsymbol{n}_{\text{eng}}$ of the engine axis, and V_{nz} and p_{nz} are the velocity and static pressure of the duct stream in a metering nozzle.

The aerodynamic characteristics of the model, which were obtained from the test results taking into account the duct-effect correction in the form of Eq. (4), have the following expansion:

$$\boldsymbol{R}_a = \boldsymbol{R}_{\text{ext}} + \boldsymbol{R}_{\text{ss}} + \boldsymbol{I}_\infty \cdot (\boldsymbol{n}_{\text{nz}} - \boldsymbol{n}_\infty) \tag{5}$$

where $\boldsymbol{R}_{\text{ext}}$ is the vector of the resultant force over the external surfaces of the airplane and the engine nacelle, which are not wetted by the airstream captured by the inlet. As stated earlier, this resultant force, in the aerodynamic data presented, includes the force $\boldsymbol{R}_{\text{base}}$ of base pressure acting over that part of the rear face of the lifting body and engine nacelle that is not occupied by the metering nozzles. The reciprocal of the x component $\boldsymbol{R}_{\text{base}}$ is usually called base drag. The vector $\boldsymbol{R}_{\text{ss}}$ is the resultant force over a so-called nonsolid streamsurface of the inlet. This streamsurface is formed by streamlines of the inlet-captured airstream passing through the leading edges of the inlet and corresponds to a portion of this stream between the freestream cross section and the inlet edges. The drag component of the $\boldsymbol{R}_{\text{ss}}$ force is also known as ram or preentry drag. The vector $I_\infty(\boldsymbol{n}_{\text{nz}} - \boldsymbol{n}_\infty)$ refers to deflection-caused forces mentioned earlier; they are a result of deflection of the airstream captured by the inlet and passing through the duct from the freestream direction $\boldsymbol{n}_\infty$ to the direction $\boldsymbol{n}_{\text{nz}}$. Note, the resultant aerodynamic force [Eq. (5)] does not include forces acting on the forebody surface wetted by the inlet-captured airstream, that is, the resultant aerodynamic drag of the ducted model does not include viscous and wave drag from the forebody surface compressing the inlet flow.

Thus, the characteristics of the inlet integrated in the vehicle system, Eqs. (1) and (2), and the total aerodynamic characteristics, Eqs. (3–5), were obtained from testing the ducted model under consideration.

Determination of the Resultant Aeropropulsive Characteristics

In this work, apart from consideration of the aerodynamic characteristics already mentioned, we performed a more detailed analysis of the properties of the examined scramjet-powered vehicle as a whole, extending the approach,[9] which implies consideration of all forces acting on the vehicle including the propulsion unit. For this purpose, estimates of the resultant aeropropulsive forces for the test Mach numbers were obtained using experimentally determined aerodynamic characteristics and flow-rate factor, as well as engine thrust characteristics calculated on the basis of one-dimensional treatment of the flow with heat addition from fuel burning in the engine combustion chamber.

The aerodynamic characteristics of ducted models obtained experimentally should be incorporated into the total forces acting on the vehicle, including all of the external and internal surfaces of the airplane and propulsion unit, in the form

$$\boldsymbol{R} = \boldsymbol{R}_a + \boldsymbol{T} \tag{6}$$

where $\boldsymbol{R}$ is the vector of the resultant aeropropulsive force over all external and internal surfaces of the airplane and engine nacelle. The lift and drag components of the resultant aerodynamic force $\boldsymbol{R}_a$ for a full-scale vehicle should be determined through nondimensional aerodynamic coefficients obtained experimentally. The engine thrust vector $\boldsymbol{T}$ should be determined in a different manner, depending on the method of duct force decomposition as mentioned earlier. When experimental determination [Eq. (5)] of aerodynamic forces corresponding to Ref. 19 are taken into account, the thrust vector in Eq. (6) should be represented in the following form:

$$\boldsymbol{T} = -(I_{\text{nze}} - I_\infty)\cdot \boldsymbol{n}_{\text{eng}}$$

$$I_{\text{nze}} = [m_{\text{nze}} V_{\text{nze}} + (p_{\text{nze}} - p_\infty) A_{\text{nze}} - m_\infty V_\infty] \tag{7}$$

where m_{nze}, V_{nze}, and p_{nze} are the mass flow rate, velocity, and static pressure of the exhausted jet and A_{nze} is the exit area of the nozzle of a full-scale engine whose thrust vector is directed along the axis $\boldsymbol{n}_{\text{eng}}$ common to the nozzle and engine. Note that the exit area of the engine nozzle of the vehicle considered refers to the total area of the base face of the lifting body and engine nacelle; thus, this relative area is $A_{\text{nze}}/A_0 = 3.78$–$4.02$ depending on the height of the diverter wedges. The flow-rate characteristics of the engine, that is, the quantity m_∞ in Eq. (7), should be determined taking into account the flow-rate factor of the inlet [Eq. (2)] obtained experimentally; the quantity m_{nze} follows from adding to m_∞ some mass of fuel supplied into the engine combustor.

The definitions and decomposition of forces used are shown in Fig. 3, which shows schematics of a ducted model in a longitudinal

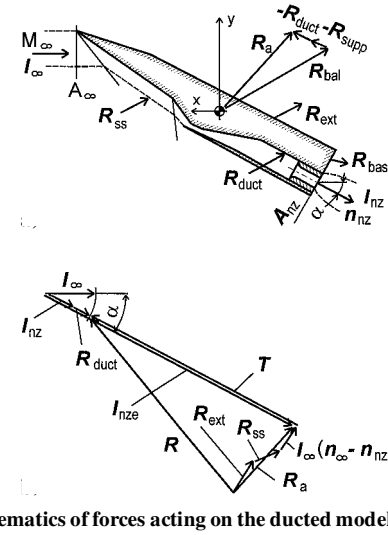

Fig. 3 Schematics of forces acting on the ducted model and airbreathing vehicle.

section (Fig. 3a) and an appropriate vector diagram (Fig. 3b). The same considerations could be applied to aerodynamic and thrust moments of the model and full-scale vehicle, but they are not involved here.

To calculate the thrust characteristics of the engine, we estimated the parameters of a one-dimensional flow in the inlet throat. The Mach number M_{th} was obtained from the equation of mass flow continuity using experimental values of the flow-rate factor,

$$q(M_{\text{th}}) = \frac{q(M_\infty) \cdot f}{\bar{A}_{\text{th}} \cdot \sigma_{\text{th}}} \tag{8}$$

where $\sigma_{\text{th}} = p_{0\text{th}}/p_{0\infty}$ is the total-pressure recovery factor of the throat flow, $\sigma_{\text{th}} = \sigma_{\text{en}}\sigma_{\text{int}}$, where $\sigma_{\text{en}} = p_{0\text{en}}/p_{0\infty}$ is the total-pressure recovery factor of the inlet-captured airstream in the entrance cross section and $\sigma_{\text{int}} = p_{0\text{th}}/p_{0\text{en}}$ is the total-pressure recovery factor for the internal flow in the inlet input section between the entrance and throat cross sections.

The values of σ_{en} were determined by calculation of the inviscid flow over the compression surfaces of the forebody and the inlet. The flow parameters near the triangular precompression surface of the forebody were found using an approximate method,[20] which presents an adaptation of the well-known tangent-wedge and tangent-cone methods as applied to triangular wing-shaped bodies. In this method, the flow near a triangular flat surface is assumed to be uniform, and its parameters are determined by interpolation between two values calculated for tangent wedge and cone, with taking into account sweep and incidence angles of the surface. Analytical formulas were used: exact for the wedge[21] and approximate for the cone.[22] The flow over the inlet wedge ramp and shock waves on its wedges were assumed to be planar. The geometry of the model inlet entrance is simple, so that the total pressure loss in the entrance section is mainly produced by an oblique shock wave arising on the cowl lip, where a supersonic flow at the entrance deflects from its direction along the wedge ramp (with an angle $\theta_3 = 22.5$ deg) to the direction in the throat ($\theta_{\text{th}} = 0$ deg). Consequently, the value $\sigma_{\text{int}} = \sigma_{\text{sw}} = p_{0\text{sw}}/p_{0\text{en}}$ was taken.

The change in the total-pressure recovery factor of the inlet-captured airstream includes some losses caused the boundary layer. In accordance with Ref. 1, if there is no shock-induced separation of the boundary layer at the inlet entrance, these losses can be estimated by the value $\sigma_{\text{bl}} = (1 - A^*_{\text{en}}/A_0)$, where A^*_{en} is the area covered by the boundary-layer displacement thickness δ^* in the inlet-entrance cross section. The value σ_{bl} was not obtained in the experiments and calculations, but these losses for a full-scale vehicle are small in comparison with the total pressure losses in the shock waves estimated by the value σ_{sw} defined earlier, and they were neglected in thrust estimations. The remaining parameters of the inlet throat flow are evident from known M_{th} and σ_{th}, and the engine thrust can be calculated.

Thus, the change in the total-pressure recovery factor of the inlet caused by the examined factors (wedge-diversion effects, presence or absence of the side cheeks, and nose bluntness) is not taken into account in estimating the throat flow parameters. Correspondingly, the calculated change in the thrust coefficient depending on these factors is related mainly to the change in the flow-rate factor obtained experimentally.

In accordance with Eqs. (6) and (7), the coefficients of tangential (directed against the freestream flow) C_{R_x} and lifting C_{R_y} components of the resultant aeropropulsive force $\boldsymbol{R}$ are determined as

$$C_{R_x} = C_T \cdot \cos(\alpha) \cdot A_0/S_{\text{pl}} - C_D$$

$$C_{R_y} = C_T \cdot \sin(\alpha) \cdot A_0/S_{\text{pl}} - C_L \tag{9}$$

where C_D and C_L are coefficients of the drag $D = -R_{a_x}$ and lift $L = R_{a_y}$ components of the aerodynamic force $\boldsymbol{R}_a$ determined experimentally in the form of Eq. (3) C_T is the coefficient of the engine thrust value $|\boldsymbol{T}|$ determined in accordance with Eq. (7).

Determining the aeropropulsive characteristics of the examined vehicle configuration as a whole means actually going from the model to a full-scale vehicle, and it should include extrapolation of experimental aerodynamic characteristics to flight conditions. It could be suggested that the change in these characteristics is mainly determined by the change in friction drag with increasing the Reynolds numbers to flight values; thus, the overall drag coefficient will decrease and improve the aerodynamic characteristics. It is difficult to separate the wave and friction drag in experimental data obtained; therefore, the said extrapolation was not performed.

A scramjet operation regime with a supersonic velocity in the combustion chamber was examined for the propulsion unit of the full-scale vehicle considered. In determining the thermogasdynamic and thrust characteristics of the scramjet, we used a simplified approach whose brief description and main assumptions can be found in Refs. 23 and 24. The approach was based on Refs. 25–28. Flight Mach numbers corresponded to the test Mach numbers, and the other flight conditions were considered corresponding to a dynamic pressure $q_\infty = 7 \times 10^4$ N/m^2 ($p_\infty = 6.25 \times 10^3$ N/m^2, $t_\infty = 216.65$ K for $M_\infty = 4$ and $p_\infty = 2.78 \times 10^3$ N/m^2, $t_\infty = 221$ K for $M_\infty = 6$). The relative throat area $\bar{A}_{\text{th}} = 0.12$ was preset for an inlet of the full-scale vehicle, and the throat flow parameters were calculated from Eq. (8). The scramjet operation mode with supersonic combustion and with fuel supply corresponding to the air-to-fuel ratio $\alpha_{\text{af}} = 1$ was assumed. An initial fuel portion was supplied in the combustion section of constant cross-sectional area $A_{\text{ch}}/A_{\text{th}} = 1.5$; the possible amount of injected fuel was determined from the condition of reaching the critical velocity $M_{\text{ch}} = 1.0$ at the exit of this section. An additional fuel portion was supplied in the next flared combustion section to reach the given air-to-fuel ratio $\alpha_{\text{af}} = 1$. The condition $M_{\text{ch}} = \text{const} = 1.0$ was held for this process. The engine jet expanded adiabatically in an exhaust nozzle from a cross-sectional area corresponding to the fuel supply completion up to the nozzle exit cross-sectional area $A_{\text{nze}}/A_0 = 3.78$–$4.02$ mentioned earlier.

A calorific value $H_u = 1.3 \times 10^8$ J/kg and a stoichiometric mass air-to-fuel ratio $L_0 = 34.25$ were taken for the fuel (gaseous hydrogen). The specific gas constant of combustion products was determined as $R_{\text{cp}} = (R_{\text{air}}\, m_\infty + R_{\text{fuel}}\, m_{\text{fuel}})/(m_\infty + m_{\text{fuel}})$. The heat capacity of the combustion products was assumed to be constant and characterized by the effective ratio of specific heats $\gamma_{\text{cp}} = 1.26$ accepted by Ref. 25. The combustion efficiency and other coefficients that specify losses of different kinds in the combustor and in the nozzle were assumed to be equal to unity, that is, the thrust estimates obtained correspond, in a certain sense, to ideal characteristics of the scramjet.

Note that the contribution of the engine thrust to the lift force of the vehicle is rather small despite its reasonably large motorization factor. The latter can be characterized by the relative cross-sectional areas of the input and output units of the engine, of the inlet $A_0/S_{\text{pl}} = 0.026$ and of the nozzle $A_{\text{nze}}/S_{\text{pl}} \approx 0.1$. This is appreciably explained by the engine thrust being aligned with the construction axis of the engine and the vehicle by presumption, that is, the lift and tangential thrust components are merely $C_{T_y} = C_T \sin(\alpha)$ and $C_{T_x} = C_T \cos(\alpha)$.

Boundary-Layer Diversion

Effects of boundary-layer diversion were experimentally studied for a configuration of the model on which the pointed nose of the lifting body and the engine nacelle variant with the noncheeked inlet were mounted. The schlieren pictures of the flow pattern over the external compression section of the inlet were obtained in these experiments. They showed that, within almost the entire range of the angle of attack under study, a supersonic inflow at the inlet duct entrance occurs for the model variant without diverter wedges both for $M_\infty = 6$ and for $M_\infty = 4$. A shock wave detached from the leading edge of the inlet cowl was observed for angles of attack $\alpha > 9$ deg in tests of the model variant with wedges $h_{\text{blw}} = 3.7$ mm at $M_\infty = 4$. Thus, regimes of the flow around the inlet with a supersonic inflow at the entrance and a supersonic flow in the throat were mainly obtained in the experiments.

To choose properly the required heights of diverter wedges, one should know the boundary-layer parameters ahead of the inlet. The

state of the boundary layer developed on the forebody compression surface was estimated on the basis of transition data obtained by V. I. Kornilov (unpublished, private communication) for a flat plate tested in the T-313 wind tunnel for $M_\infty = 2.5$–6 and different Reynolds numbers per meter. The transition Reynolds numbers obtained obey the power dependence $Re_{tr} \sim Re_{1\infty}^{n}$ with an exponent $n \approx 0.4$ extended for the T-313 wind tunnel in Ref. 29 by data for $M_\infty = 3$ and 4. The effect of the sweep angle χ was taken into account by data[30] for triangular flat wings also tested in T-313 at $M_\infty = 3$ and 4. According to these data, the relationship $(Re_{tr})_{\chi \neq 0}/(Re_{tr})_{\chi = 0}$ changes little as compared between $M_\infty = 3$ and 4, and the said ratio determined for $M_\infty = 4$ was extended to $M_\infty = 6$. For experimental conditions under consideration, $\alpha = 0$, the following values of the Reynolds number and the length of the boundary-layer transition on the nose swept compression surface were estimated: $M_\infty = 4$, $Re_{tr} = 3.8$–5.7×10^6, and $L_{tr} = 19$–29 mm, and $M_\infty = 6$, $Re_{tr} = 5.9$–8.6×10^6, and $L_{tr} = 83$–120 mm. Thus, a developed turbulent boundary layer was expected immediately in front of the inlet wedge, which corresponds to flight flow conditions of full-scale hypersonic aircraft.

For the model under consideration, the characteristics of the boundary layer on the precompression surface of the forebody were experimentally derterminedⁿ in the plane of symmetry $z = 0$ at a distance $x = 340$ mm from the nose tip of the model. The static pressure on the wall and the pitot-pressure profile in the boundary layer were measured with a small-size probe positioned on a traversing gear. The velocity distribution in the boundary-layer, the boundary-layer thickness δ, the displacement thickness δ^*, and the momentum thickness δ^{**} were obtained from these data. Therewith, Crocco's integral was assumed to be valid for the description of temperature variation across the boundary layer. The boundary layer on the model surfaces developed naturally under near adiabatic temperature of the model wall $t_w \approx t_{0\infty} \approx 295$ K. The freestream parameters corresponded to Mach numbers $M_\infty = 2.03$, 3.03, and 4.05 ($Re_{1\infty} = 27 \times 10^6$, 37×10^6, and 56×10^6 1/m, respectively).

Some integral characteristics of the boundary layer on the forebody precompression surface, which will be used subsequently, were estimated under the assumption that this boundary layer is two dimensional and fully turbulent. We used the method of Ref. 31 developed as applied to the turbulent boundary layer of a nonthermoinsulated flat plate. This method presents an analytical formulation based on the logarithmic law for the velocity profile of the compressible turbulent boundary layer. Integral parameters of the boundary layer such as the thickness, displacement thickness, and momentum thickness are determined. In due course, Kovalenko[31] has demonstrated that the analytical method yields somewhat better accuracy in comparison with the well-known semi-empirical prediction procedure of Ref. 32. Note, the flow about the model forebody is, in general, three dimensional. In addition, the boundary layer over the model is really transitional, but the lengths of laminar and transitional sections of it were not determined. Thus, the said estimates cannot be rigorously correlated with the experimental data obtained, but they give some reference estimates. In particular, they allowed the choice of diverter wedge heights.

As is shown in Ref. 9 by analysis of the measured velocity profiles, the boundary layer ahead of the inlet is turbulent in the entire range of experimental freestream parameters considered. The integral characteristics of the boundary layer are plotted in Fig. 4 as functions of M_∞. It is evident from these data that the shape factor at $M_\infty = 4$ is about $H_{bl} = 7.8$–7.9, which corresponds to a developed turbulent boundary layer. A calculated estimate for $M_\infty = 4$ yields $H_{bl} \approx 8.1$, which conforms to the experimental value. Note that the difference in the values of δ, δ^*, and δ^{**} measured for an angle of attack $\alpha = 3$ deg does not exceed 6% in comparison with $\alpha = 0$. However, for $\alpha = 10$ deg, this difference increases appreciably and, for example, reaches ~35% for the displacement thickness δ^*.

According to the measurement data, the boundary-layer thickness δ ahead of the inlet is ~3.9 mm for $M_\infty = 4$ and $\alpha = 0$, the relative values are correspondingly $h_{blw}/\delta \approx 0.51$ for $h_{blw} = 2$ mm and $h_{blw}/\delta \approx 0.95$ for $h_{blw} = 3.7$ mm. For $M_\infty = 6$, the calculated

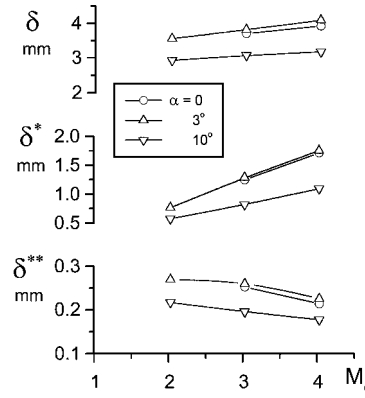

Fig. 4 Integral characteristics of the boundary layer measured on the forebody precompression surface as functions of M_∞.

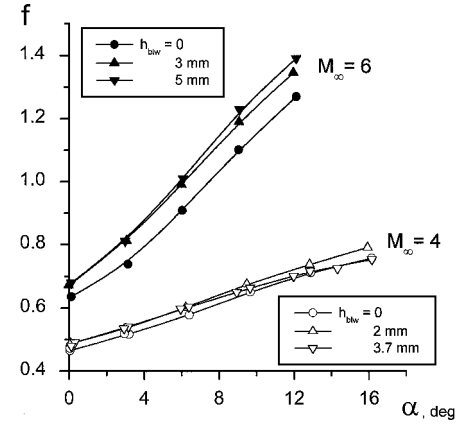

Fig. 5 Flow-rate factor of the model inlet vs the angle of attack for a set of diverter wedge heights.

boundary-layer thickness ahead of the inlet could reach $\delta \approx 5$ mm, which was confirmed by the schlieren pictures of the flow pattern around the model inlet. Hence, for the chosen heights of the diverter wedges, their expected relative heights for this Mach number are about $h_{blw}/\delta \approx 0.6$ for $h_{blw} = 3$ mm and $h_{blw}/\delta \approx 1$ for $h_{blw} = 5$ mm. Taking into account the high-power character of velocity distribution in the turbulent boundary layer, we may assume that the values $h_{blw}/\delta \geq 0.5$–0.6 obtained for the model will allow elimination of the influence of its most stagnated part and a tangible increase in the inlet efficiency.

Let us consider the effect of wedge diversion of the boundary layer on the flow-rate characteristics of the inlet. The experimental values of the flow-rate factor f are plotted in Fig. 5 for Mach numbers $M_\infty = 4$ and 6 as functions of the angle of attack. The data for the examined values of the diverter wedge height h_{blw} are presented. As evident from these data, an increase in the relative height of the diverter wedges above $h_{blw}/\delta \geq 0.5$–0.6 weakly affects the flow-rate factor. The schlieren pictures show that, for $M_\infty = 4$, $h_{blw} = 3.7$ mm and $M_\infty = 6$, $h_{blw} = 5$ mm, the near-wall stagnated part of the boundary layer developed on the forebody surface passes through the slot for boundary-layer diversion. That is, the flow around the inlet ramp is affected only by the external, dynamic part of the viscous layer. Under these conditions, a new boundary layer is developed on the inlet wedge ramp. The thickness of this new boundary layer at the inlet entrance cross section is much smaller than that occurring for the model variant without the diverter wedges. For instance, based on the data of the schlieren pictures, we can say that the thickness of the boundary layer in the inlet entrance cross section for a Mach number $M_\infty = 6$ in the absence of its diversion is more than 50% of the entrance height; with the diverter wedges of height $h_{blw} = 5$ mm, this thickness decreases to about 25%.

The specific behavior of the flow-rate factor as a function of the angle of attack for $\alpha > 6$ deg in model testing with $M_\infty = 4$ and the wedge height $h_{blw} = 3.7$ mm ($h_{blw}/\delta \approx 1$) should be noted (see Fig. 5). Despite that the boundary layer ahead of the inlet is almost

completely cut off, the flow-rate factor has lower values as compared to the wedge with $h_{blw} = 2$ mm ($h_{blw}/\delta \approx 0.51$). For $\alpha > 14$ deg, this factor becomes almost equal to that for the variant without boundary-layer diversion $h_{blw} = 0$. The schlieren pictures show that, in this range of flow parameters at the inlet entrance, there is a shock wave detached from the leading edge of the cowl. Note that the wedges with $h_{blw} = 3.7$ mm provide the passage of practically all of the boundary layer developed on the forebody under the inlet ramp ($h_{blw}/\delta \approx 0.95$). The calculated estimates for an inviscid flow in this case also indicate the possibility of this detachment due to the excess of the critical angles of flow deflection on the cowl. At the same time, no detached shock wave was observed in the case of wedges with $h_{blw} \leq 2$ mm, apparently, because of a certain reconstruction of the flow pattern with a rather thick boundary layer. As a whole, we can note that, up to angles of attack corresponding to the maximum lift-to-drag ratio $\alpha_{(L/D)max} \approx 6$ deg, an increase in the wedge height above $h_{blw}/\delta > 0.5$–0.6 does not lead to a further significant increase in the flow-rate factor and does not seem reasonable. For angles of attack close to $\alpha_{(L/D)max}$, the flow-rate factor increases by ~5 and ~11% for $M_\infty = 4$ and 6, respectively, which, obviously, leads to an increase in the thrust produced by the propulsion unit.

The drag of the vehicle as a whole, in a configuration with wedges for boundary-layer diversion, should increase through the wave drag and friction drag of the wedges themselves, friction drag of additional wetted surfaces in the slot for boundary-layer diversion between the engine nacelle and the body, and also interference drag. Obviously, for a ducted model with such wedges tested with the use of the experimental technique discussed earlier, the drag over the inlet streamsurfaces should also change as a consequence of changing the flow-rate factor as compared to its variant without wedges. The drag coefficient C_{D_0} of the model as a function of the wedge height is shown in Fig. 6. An increase in the value of C_{D_0} by 20–26% for a Mach number $M_\infty = 4$ and by 27–32% for $M_\infty = 6$ is observed as compared to the case $h_{blw} = 0$. These data show that the relative contribution of the wedges to the drag somewhat increases with increasing freestream Mach number.

An analysis of the lifting properties of the hypersonic vehicle configuration considered showed[9] that, within the range of the angles of attack $\alpha = 0$–12 deg, the presence of the diverter wedges involved a small increase in the lift coefficient C_L for $M_\infty = 6$ and had practically no effect on it for $M_\infty = 4$. The dependences of the lift-to-drag ratio L/D vs the angle of attack for $M_\infty = 6$ and for the studied

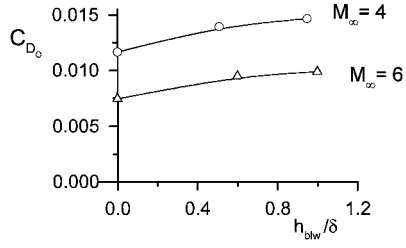

Fig. 6 Drag coefficient of the model at zero lift vs the relative diverter wedge height.

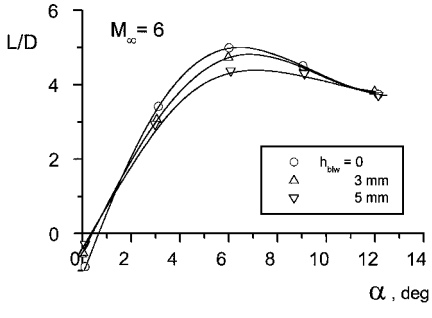

Fig. 7 Lift-to-drag ratio as a function of the angle of attack for a set of diverter wedge heights.

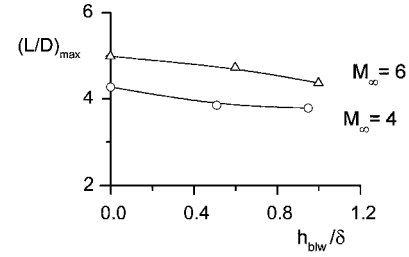

Fig. 8 Maximal lift-to-drag ratio vs the relative diverter wedge height.

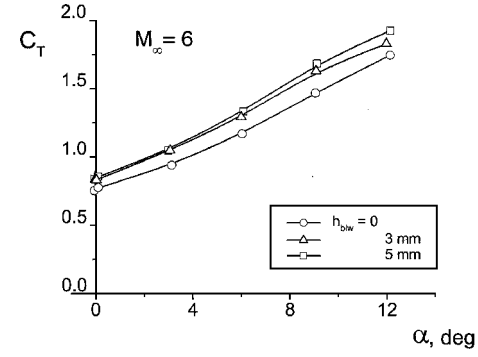

Fig. 9 Engine thrust coefficient vs the angle of attack for $M_\infty = 6$ and for a set of diverter wedge heights.

set of values of h_{blw} and the maximal lift-to-drag ratio $(L/D)_{max}$ vs the wedge height h_{blw} are plotted in Figs. 7 and 8, respectively. The decrease in $(L/D)_{max}$ caused by the presence of diverter wedges amounts up to 12% as compared to the variant without boundary-layer diversion.

The discussed experimental data demonstrate that, despite the improvement of the flow-rate characteristics of the inlet, the presence of wedges for boundary-layer diversion leads to a noticeable increase in the drag of the vehicle as a whole and, hence, to a decrease in the maximal lift-to-drag ratio. At the same time, it is obvious that these data are insufficient for making the final conclusion about the efficiency of boundary-layer diversion. Analysis of all of the forces acting on the vehicle including the propulsion unit is needed to evaluate such a global efficiency. As has been mentioned, such an analysis for the hypersonic vehicle under study was carried out using estimates of the resultant aeropropulsive forces, which were obtained by combining the aerodynamic characteristics determined experimentally and the thrust characteristics of the scramjet engine calculated by approximate methods.

As has been described, calculation of the engine thrust proceeds from flow parameters in the inlet throat, which mainly depend on the flow-rate factor obtained experimentally. By calculation, the pressure recovery factor and Mach number in the throat are $\sigma_{th} = 0.73$–0.76 with $M_{th} = 2.25$–1.75 at $M_\infty = 4$ and $\sigma_{th} = 0.51$–0.56 with $M_{th} = 3.25$–2.52 at $M_\infty = 6$. Thus, the pressure recovery factor varies little with the angle of attack.

The engine thrust coefficient for $M_\infty = 6$ is presented in Fig. 9 vs the angle of attack $C_T(\alpha)$. For the configuration with diverter wedges $h_{blw} = 5$ mm (corresponding to $h_{blw}/\delta \approx 1$), the thrust coefficient increases by 9–11% as compared to the variant $h_{blw} = 0$. This increase is caused by the increase in the flow-rate factor, which results from the mentioned simplified determination of the flow parameters in the inlet throat and, respectively, the engine thrust. The estimated effect of boundary-layer diversion on the scramjet thrust is in agreement with the data of Ref. 8, where the same effect was calculated taking into account the displacing action of the boundary layer.

The resultant aeropropulsive characteristics for $M_\infty = 6$ are illustrated in the form of polars: dependences $C_{R_y}(C_{R_x})$ plotted in Fig. 10. The aerodynamic polars $C_L(C_D)$ are also presented in Fig. 10. The greatest relative increment in the drag caused by the

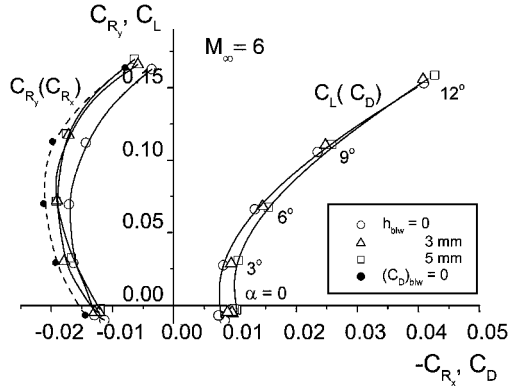

Fig. 10 Polars of aerodynamic forces $C_L(C_D)$ and resultant aeropropulsive forces $C_{R_y}(C_{R_x})$ for $M_\infty = 6$ and for a set of diverter wedge heights.

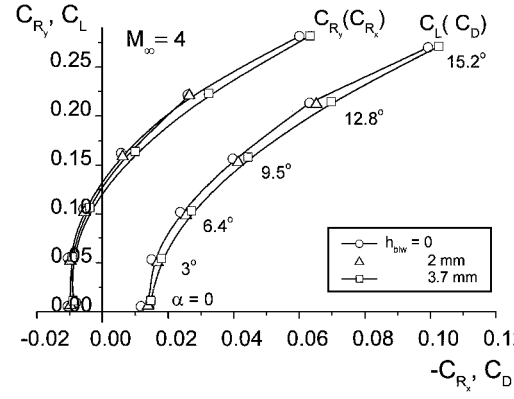

Fig. 11 Polars of aerodynamic forces $C_L(C_D)$ and resultant aeropropulsive forces $C_{R_y}(C_{R_x})$ for $M_\infty = 4$ and for a set of diverter wedge heights.

diverter wedges is observed near $\alpha = 0$; therewith the resultant tangential force remains virtually unchanged. A significant increment in the coefficient C_{R_x} of this force occurs for $\alpha > 6$ deg ($C_{R_y} > 0.06$), and it is almost the same for $h_{\text{blw}} = 3$ mm ($h_{\text{blw}}/\delta = 0.6$) and $h_{\text{blw}} = 5$ mm ($h_{\text{blw}}/\delta = 1.0$).

It is obvious that this positive effect can be enhanced by optimization of the wedges for boundary-layer diversion. For instance, the experimental data presented allow one to estimate the resultant characteristics corresponding to zero drag of the diverter wedges $(C_D)_{\text{blw}} = 0$, which in a certain sense corresponds to bleeding the boundary layer developed upstream of the inlet. The values of the flow-rate factor for the greatest height of the wedges ($h_{\text{blw}} = 5$ mm for $M_\infty = 6$) and aerodynamic characteristics for the model variant without the wedges ($h_{\text{blw}} = 0$) can be used for this purpose. A dashed curve connecting the solid circles in Fig. 10 shows these estimates. For this case, there is an increase in the resultant tangential force over the entire range of angles of attack examined. However, note that these estimates can be considered only as a limit for the aeropropulsive characteristics that could be reached due to boundary-layer suction upstream of the inlet. A more rigorous estimate of the efficiency of such boundary-layer bleeding requires the energy losses on suction to be taken into account, including the effect of dumping the bled air back into the engine duct stream.

The following distinctive feature of the polars of the resultant aeropropulsive forces presented in Fig. 10 should be noted. The tangential force increases with increasing the lift force or with changing the angle of attack from $\alpha = 0$ to $\alpha \approx 6$ deg, and thereafter it begins to decrease. The initial increase in this force is a result of the significant increase in the inlet flow-rate factor with increasing the angle of attack; the engine thrust rises, correspondingly, approximately linearly (see Fig. 9). This increase in the propulsive force exceeds that for aerodynamic drag. For $\alpha > 6$ deg, the further increase in the inlet flow-rate factor and engine thrust does not compensate the drag rising approximately as the angle of attack squared. Corresponding to the behavior of C_{R_x} as a function of C_{R_y}, two branches, respectively, the lower and the upper ones, can be distinguished, which differ by the aircraft response to a perturbation of the angle of attack at a given flight Mach number. For instance, for flight values C_{R_y} corresponding to the upper branch of the polar, a perturbation increasing the angle of attack should be accompanied by an ordinary response: transition to a decelerated climb. For the lower branch of the polar, such a perturbation should be accompanied by the transition from a steady horizontal flight or a steady climb flight to a spontaneously accelerated climb. This sort of path instability was discussed in Refs. 23 and 24; obviously, it correlates with the conventional characteristics of aircraft such as the speed stability and the stability related to the angle-of-attack load.

The calculated resultant aeropropulsive characteristics of scramjet-powered aircraft presented in Refs. 23 and 24 show that the said feature of the resultant polar is representative of aircraft configurations with a scramjet module positioned under the lifting body. Note that conventional flight conditions of hypersonic aircraft correspond to dynamic pressures $q_\infty = 5$–8×10^4 N/m^2 and $C_{R_y} = 0.05$–0.1. In the case $M_\infty = 6$ considered, these flight parameters will fall onto the lower unstable branch of the polar.

Related estimates of the resultant aeropropulsive forces were obtained for $M_\infty = 4$ (see Fig. 11). They showed that there is scarcely any effect of the diverter wedges on increasing the resultant tangential force in this case. Taking into account the approximation of engine thrust calculations, one can say that the wedges for boundary-layer diversion in this case at least do not worsen the aircraft performance. Also note that the resultant polars $C_{R_y}(C_{R_x})$ for $M_\infty = 4$ have no unstable branch, that is, they are characterized by the ordinary response to perturbations over the entire range of the angle of attack considered. Such a change in the form of the resultant polars for $M_\infty = 4$ as compared to $M_\infty = 6$ is also associated[23] with path instability analogous to that discussed earlier.

As a whole, the presented experimental results and calculation estimates on effects of wedge-aided diversion of the boundary layer showed that mounting the inlet on such wedges of an appropriate height allows reaching, at high Mach numbers, some increase in the total propulsive force of the vehicle despite the increase in the drag force. This supports the conclusions[8] obtained only on the basis of calculation estimates. To determine the benefits of arrangement of diverter wedges on a certain hypersonic vehicle, obviously, it is necessary to take into account the influence of other factors, for example, the angles of the wedges and their longitudinal contour, the sweep angles and the bluntness of their leading edge, etc. Some optimization and improvement of the characteristics of the wedges is also possible. Also bear in mind that the characteristics of devices for boundary-layer diversion depend on the particular arrangement of the propulsion unit on the vehicle. Therefore, it is desirable to perform more complete investigations of the influence of various factors on the efficiency of boundary-layer diversion for particular conditions.

Effect of Lateral Spillage over the Compression Wedge Ramp of the Inlet

A configuration of the model with a pointed nose and without diverter wedges was used for experimentation to compare the engine nacelle variants with the cheeked and noncheeked inlets. The effects of lateral spillage for a two-dimensional inlet with or without side cheeks depending on M_∞ should be considered by taking into account the design Mach number of the inlet M_d. For Mach numbers $M_\infty < M_d$ or for $M_\infty = M_d$ and $\alpha > 0$, the cheeks only partially restrict the region of flow over the compression ramp behind the shock waves from the external flow on the sides of the inlet. As a consequence, lateral spillage is observed even in the presence of the cheeks, which can lead to a change in the inlet characteristics, in particular, in the flow-rate factor. Obviously, the effects of lateral spillage should depend on the width-to-length ratio of the

inlet ramp related directly to the width-to-height ratio of the inlet $b_{\text{inl}}/h_{\text{inl}}$.

Effects of lateral spillage were studied, for instance, in Ref. 2. A flat inlet defined by $M_d = 5.3$, a three-wedge ramp of $\theta_1 = 7.5$, $\theta_2 = 15$, and $\theta_3 = 27.5$ deg and $b_{\text{inl}}/h_{\text{inl}} \geq 4$ was considered; it was located under a delta wing. It was shown that the presence of the side cheeks increased the flow-rate factor only by 1.5–2% for $M_\infty \leq M_d$ and by 2–3% for $M_\infty > M_d$ as compared with the noncheeked inlet variant. However, a more pronounced effect of the side cheeks was revealed,[10] for an inlet with $M_d = 4$, a two-wedge ramp of $\theta_1 = 12$ and $\theta_2 = 22.8$ deg, and $b_{\text{inl}}/h_{\text{inl}} = 1.33$. For this inlet, the presence of the side cheeks led to an increase in the flow-rate factor, essentially at M_∞ close to the design M_d. For $M_\infty = 4 = M_d$ and $\alpha = 0$, this increase accounted for about 22%. Similarly, an increase of about 11% in the flow-rate factor caused by the presence of the side cheeks was observed[11] for an inlet with a one-wedge ramp of $\theta_1 = 10$ deg, $b_{\text{inl}}/h_{\text{inl}} = 1$ in the design flow regime $M_\infty = M_d = 6.1$. Note that the data[10,11] refer to two-dimensional inlets nonintegrated with a forebody, that is, outside of their arrangement on an airplane. An inlet integrated with the airplane experiences the action of a three-dimensional flow from the forebody. For instance, despite that the lower surface of the model forebody is freestream directed in the case $\alpha = 0$, the upper and side surfaces are inclined relative to the freestream, and the flow over them is compressed. There is some cross overflow from the upper side to the lower surface caused by this compression, which involves a change in flow parameters ahead of the inlet and leads, in particular, to an off-design flow regime for it. The said cross overflow acts in a direction opposite to the lateral spillage over the inlet ramp, so that one might expect that the effects of lateral spillage related to the presence or absence of the side cheeks in this case will be manifested to a smaller extent as compared to nonintegrated inlets.

The experimental data obtained for $M_\infty = 4$ and 6 on the flow-rate factor of the inlet for the examined model configuration with pointed nose are plotted in Fig. 12, where the model variant with the inlet cheeked engine nacelle is compared with the noncheeked variant. The increment in the flow-rate factor Δf caused by the side cheeks does not exceed 1.2–2.8% for $\alpha = 0$ and decreases with increasing angle of attack. Thus, the efficiency of the side cheeks in restriction of lateral spillage of the ramp-compressed flow corresponds to that noted previously in Ref. 2 for inlets with $b_{\text{inl}}/h_{\text{inl}} \geq 4$, although the relative width of the inlet for the model configuration tested is approximately two times smaller, $b_{\text{inl}}/h_{\text{inl}} = 1.91$. The relative increment in the flow-rate factor $\Delta f/f$ for our inlet even for $M_\infty = M_d$ is significantly smaller than the values obtained[10] for a nonintegrated inlet with $b_{\text{inl}}/h_{\text{inl}} = 1.33$, for which a substantial effect of the side cheeks in design flow regimes was noted.

In the context of consideration of lateral spillage effects at $M_\infty = M_d$, the question on the inlet design-flow pattern should be discussed. Note that this flow pattern is defined for the model inlet proper under the assumption that the flow with the design Mach number $M_d = 6$ upstream of the inlet is uniform and the flow over the inlet is two dimensional. It should occur for the cheeked inlet of the model in the case of $M_\infty = 6$ and $\alpha = 0$, where the forebody precompression surface is located along the freestream flow. The inlet flow-rate factor should be unity $f = 1$ therewith. However, the experimental flow-rate factor is significantly smaller than unity (about $f \approx 0.65$, Fig. 12).

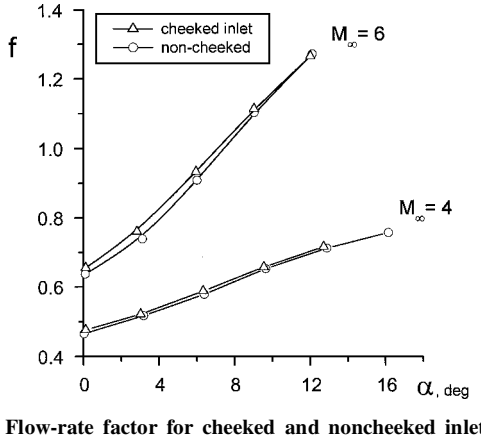

Fig. 12 Flow-rate factor for cheeked and noncheeked inlets of the model vs angle of attack.

As was noted earlier, there is some deviation of the flow pattern from the design mode one for the inlet combined with the vehicle forebody. The flow over the precompression surface formed by the forebody is three dimensional in front of the inlet even for $\alpha = 0$, and these flow parameters differ from those for the freestream flow with $M_\infty = M_d$. It is one of the factors affecting the said discrepancy of the design and real inlet flow-rate factors. However, numerical computations[33] of the flow around the configuration considered, which were performed for $M_\infty = 4$ using an Euler code, show that the said flow three dimensionality rather weakly affects the flow over the inlet itself and its flow-rate factor as compared to a purely two-dimensional flow. The values of the flow-rate factor computed for a three-dimensional flow over the forebody/inlet configuration and for a purely two-dimensional one are virtually the same for $\alpha = 0$ and differ by no more than 3.7% for $\alpha = 5$ deg.

The second essential factor is the effect of boundary-layer displacement. As was already discussed for $M_\infty = 6$ and $\alpha = 0$, the boundary layer on the wedge ramp in the inlet entrance cross section occupies more than 50% (roughly 50–70%) of the entrance height. If the boundary layer at the entrance is turbulent, its displacement thickness, by estimation in accordance with Ref. 31, will be about 13–18% of the entrance height. A decrease in the flow-rate factor caused by this displacing effect of the boundary layer is in proportion to the already mentioned area A^*_{en} as $\Delta f/f \approx A^*_{\text{en}}/A_{\text{en}}$. The value A^*_{en} for the noncheeked inlet variant is determined only by the boundary layer on the wedge ramp; for the cheeked inlet it should be greater because of the boundary layer developing on the side cheeks. The value of $\Delta f/f$ will be even somewhat greater for a certain slowdown of the inviscid flow out of the boundary layer due to its displacement effect.

The effects of flow three dimensionality and boundary-layer displacement together explain to a large extent the already mentioned discrepancy in the flow-rate factor. The displacement effect of a rather thick boundary layer may also enhance three dimensionality of the flow over the inlet, notably for its noncheeked variants.

The change in the drag coefficient C_{D_0} at a zero lifting force according to whether the side cheeks are present or absent has rather an ambiguous character depending on the freestream Mach numbers M_∞ under study. For example, for $M_\infty = 4$, the drag coefficient for the configuration variant with the inlet-cheeked engine nacelle is $C_{D_0} = 0.0129$ as compared to the noncheeked variant $C_{D_0} = 0.0117$, that is, the drag increases by ~10%. For $M_\infty = 6$, we have $C_{D_0} = 0.0065$ and 0.0073, that is, the drag coefficient decreases by roughly the same value. This behavior of C_{D_0} may be related to the corresponding change in the drag over the inlet streamsurface $C_{D_{\text{ss}}}$. The latter drag for two-dimensional inlets was numerically studied in Ref. 10, and the changes in $C_{D_{\text{ss}}}$ of the same character were obtained for the cases in the presence or absence of the side cheeks. This effect can be explained by the following. For a cheeked inlet, the area of the inlet streamsurface on the sides decreases as compared to the noncheeked variant, which leads to the corresponding decrease in $C_{D_{\text{ss}}}$, notably in the case of flow regimes close to $M_\infty \approx M_d$. Despite an additional drag of external surfaces of the side cheeks, the total drag of the configuration may become lower. For Mach numbers $M_\infty < M_d$, the arrangement of the side cheeks, that is, the restriction of lateral spillage, additionally leads to an increase in the slope of the shock waves arising on the inlet ramp. This, consequently, leads to an increase in the length and area of the inlet streamsurface and to an increase in the drag over this streamsurface. The experimental data on C_{D_0} for the vehicle configuration considered confirm the conclusion[10] made on the basis of numerical calculations of an inviscid flow that, in terms of the smaller drag, a better inlet is the inlet with complete side

cheeks for $M_\infty \approx M_d$ and the inlet with short cheeks or without them for $M_\infty < M_d$.

An analysis of the aerodynamic characteristics of the model showed that the lifting properties of the configuration and, correspondingly, the inductive drag did not practically depend on the restriction of lateral spillage on the compression ramp of the inlet. Therefore, the change in the lift-to-drag ratio L/D associated with the presence or absence of the side cheeks as a function of M_∞ is determined by the corresponding change in $C_{D_0}(M_\infty)$. The maximal lift-to-drag ratio of the configuration with the inlet-cheeked engine nacelle variant as compared to the noncheeked one for $M_\infty = 4$ is $(L/D)_{\max} = 4.03$ and 4.28, respectively, that is, it is smaller by ~4%, whereas for $M_\infty = 6$, it is greater by ~8%, $(L/D)_{\max} = 5.4$ and 5.0. For both variants of the engine nacelle, the maximal lift-to-drag ratio of the model increases with increasing the freestream Mach number.

Thus, in flow regimes with $M_\infty \approx M_d$, both the flow-rate characteristics of the inlet itself and the total aerodynamic characteristics are better for the model variant with the inlet-cheeked engine nacelle than for the noncheeked variant. The relative increase in the flow-rate factor and the decrease in drag are not large, but both characteristics are improved simultaneously, and a more noticeable increase in efficiency of the engine and the vehicle as a whole may be expected.

To evaluate the effect of the presence or absence of the side cheeks on the overall efficiency of the vehicle, the integral aeropropulsive characteristics of the configuration were considered for test Mach numbers. It was made in the same manner as for the case of the study on wedge-aided diversion of the boundary layer. The polars of the resultant aeropropulsive forces $C_{R_y}(C_{R_x})$ together with the aerodynamic polars $C_L(C_D)$ for the model tested with different variants of the engine nacelle are shown in Fig. 13 for $M_\infty = 6$. Note that the difference in the aerodynamic polars $C_L(C_D)$ for these variants is mainly manifested in a shift of one polar relative to the other because of the different values of C_{D_0}. This is because the presence or absence of the side cheeks has an insignificant effect on the lift force and lift-dependent drag of the configuration. The polars presented show that, at freestream Mach numbers close to the inlet design Mach number $M_\infty \approx M_d$, the inlet with complete side cheeks, which is better, in terms of the smaller drag, as compared to the noncheeked inlet, is also better in terms of aeropropulsive performance.

The propulsive force for the inlet-cheeked model configuration is larger in comparison to the noncheeked variant within the entire range of angles of attack considered. The increment ΔC_{R_x} in the resultant aeropropulsive force caused by the presence of the side cheeks remains almost constant within the entire range of angles of attack under study. Note that the said total increment ΔC_{R_x} can be decomposed into components caused by the increase in the flow-rate factor and by the decrease in the drag C_{D_0}, respectively. For estimation of the first effects, it is necessary to determine the resultant characteristics $C_{R_y}(C_{R_x})$ using experimental data on the flow-rate factor for the inlet-cheeked model variant and on the aerodynamic characteristics for the noncheeked variant. The corresponding polar $C_{R_y}(C_{R_x})$ is also plotted in Fig. 13 (combined data, solid circles); it differs little from the polar for configuration with the noncheeked inlet. One can see that the increase in the resultant tangential force, in this context, is predominantly associated with the decrease in the drag C_{D_0}.

The polars of the resultant aeropropulsive forces obtained for $M_\infty = 4$ and for different variants of the engine nacelle revealed that these characteristics for the cheeked inlet change very little as compared to that for the noncheeked inlet, which are presented in Fig. 11 for $h_{\text{blw}} = 0$. The resultant polars for the cheeked inlet variant, both for $M_\infty = 6$ and 4, have the same features of the path instability, which were discussed earlier for the noncheeked inlet in analyzing the effects of the diverter wedges.

Effect of Nose Bluntness of the Lifting Body

The presented results on the effect of wedge-aided diversion of the boundary layer demonstrate that the boundary layer developing on the precompression surface of the forebody and on the external compression ramp of the inlet itself is one of the main factors determining the efficiency of inlet operation for the vehicle configuration considered. In the case of the forebody with the blunted nose that forms a strong bow shock wave, a high-entropy layer develops near the body surface, which complicates development of the boundary layer. The thickness of this entropy layer may be comparable with or greater than the thickness of the viscous layer. Numerical computations[13] of the inviscid flow around a delta wing with blunted leading edges show that the thickness of the entropy layer on the lower surface related to the wing length increases with increasing Mach number M_∞ and decreases with increasing angle of attack. Note that, in most cases, it is impractical to distinguish in the near-wall flow the viscous nonuniformity related to energy dissipation in the boundary layer from the inviscid nonuniformity caused by energy dissipation in the detached curved strong shock wave. Therefore, in our work we understand the near-wall flow as the viscous–entropy layer, including both effects, under the assumption that static pressure is constant across this layer, which holds for the boundary layer.

To reveal the bluntness effect on the aerodynamic efficiency of the considered hypersonic scramjet-powered vehicle as a whole, a comparative study of the boundary layer on the precompression surface of the forebody was performed at $M_\infty = 4.05$ for model configuration variants with a pointed and blunted nose. A configuration of the model with the inlet–noncheeked engine nacelle and without wedge-aided diversion of the boundary layer was tested. As already indicated, the boundary layer was measured on the forebody

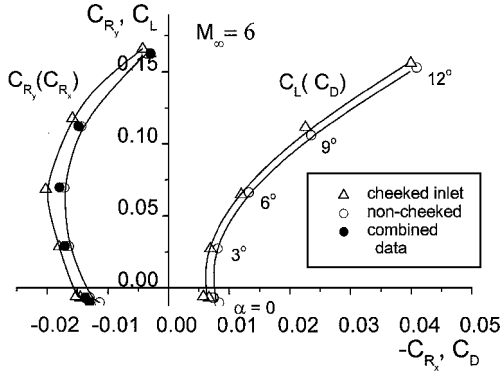

Fig. 13 Polars of aerodynamic forces $C_L(C_D)$ and resultant aeropropulsive forces $C_{R_y}(C_{R_x})$ for $M_\infty = 6$; model variants with cheeked and noncheeked inlets.

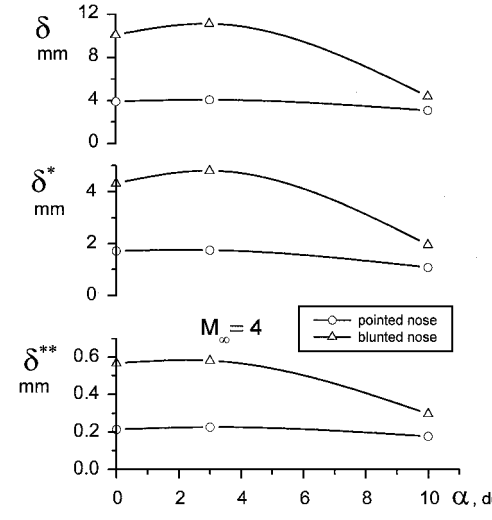

Fig. 14 Integral characteristics of the boundary layer measured in testing the model with different nose bluntness at $M_\infty = 4$.

pre-compression surface in the plane of symmetry $z = 0$ at a distance $x = 340$ mm from the model nose tip.

An example of the integral characteristics of the boundary layer measured in testing the model with different nose bluntness for $M_\infty = 4.05$ and $Re_{1\infty} = 56 \times 10^6$ 1/m is shown in Fig. 14. Note that the nose bluntness leads to a significant increase in all thickness dimensions of the boundary layer. For instance, within the range of angles of attack $\alpha = 0$–3 deg, the values of δ, δ^*, and δ^{**} increase by a factor of 2.5–2.7 and for $\alpha = 10$ deg by a factor of 1.4–1.8 as compared to the pointed configuration. An analysis of boundary-layer velocity profiles obtained for the configuration with the blunted nose showed that the entropy layer seemed to be absorbed by the boundary layer upstream of the measurement cross section only for angles of attack $\alpha \geq 10$ deg.

Based on the measurement data for $M_\infty = 4$ and $\alpha = 0$, the boundary-layer thickness ahead of the inlet for the pointed configuration is $\delta = 3.9$ mm, and the displacement thickness is $\delta^* = 1.7$ mm. In the case with nose bluntness, the corresponding values are $\delta = 10.1$ mm and $\delta^* = 4.3$ mm. This significant increase in the displacement thickness should be accompanied by noticeable losses of the flow rate of air through the inlet. The experimental values of the flow-rate factor obtained for the blunted configuration at $M_\infty = 4$ and 6 are plotted in Fig. 15 as a function of the angle of attack. For comparison, Fig. 15 also shows the data for the pointed configuration discussed earlier. For angles of attack near $\alpha = 0$, the nose bluntness decreases the flow-rate factor by ~23% for $M_\infty = 4$ and by ~42% for $M_\infty = 6$, that is, the losses of the flow rate caused by the nose bluntness significantly increase with increasing the freestream Mach number. Nevertheless, the effect of nose bluntness decreases with increasing angle of attack, as could be expected from evidence of the measured values of δ^*. For $\alpha \geq 9$ deg, the flow-rate factors for the blunted and pointed configurations are close.

The character of variation of the flow-rate factor as a function of the angle of attack for the blunted configuration determines to a large extent the behavior of the total aerodynamic characteristics of the configuration as a whole, which include the forces over the inlet streamsurface. In particular, note that, for a Mach number $M_\infty = 6$, the model drag significantly increases within the range of angles of attack $\alpha \leq 6$ deg, and the aerodynamic polar $C_L(C_D)$ for the blunted configuration is no longer parabolic (Fig. 16). The increase in the zero-lift drag coefficient C_{D_0} reaches ~12% for $M_\infty = 4$ and ~21% for $M_\infty = 6$. Thus, the effects of nose bluntness on the vehicle drag and on the inlet flow-rate factor increase with increasing freestream Mach number.

The experimental data showed that the lifting properties of the configuration depended weakly on nose bluntness, though some increase in the values C_L and C_L^α was observed within the range of angles of attack $\alpha = 0$–6 deg for $M_\infty = 6$. As a whole, nose bluntness decreased the maximal lift-to-drag ratio $(L/D)_{\max}$ by ~3% for $M_\infty = 4$ and by ~7% for $M_\infty = 6$. At the same time, because of the already noted deformation of the aerodynamic polars $C_L(C_D)$,

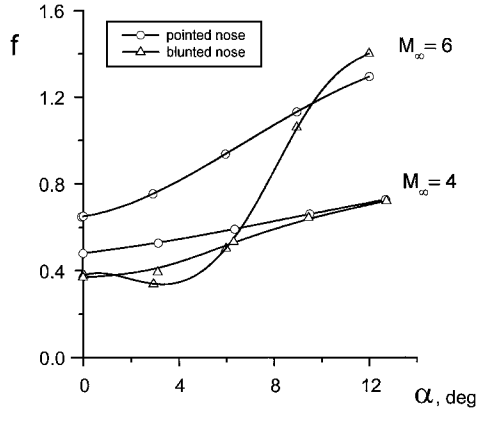

Fig. 15 Inlet flow-rate factor vs the angle of attack for the model variants with blunted and pointed nose tips.

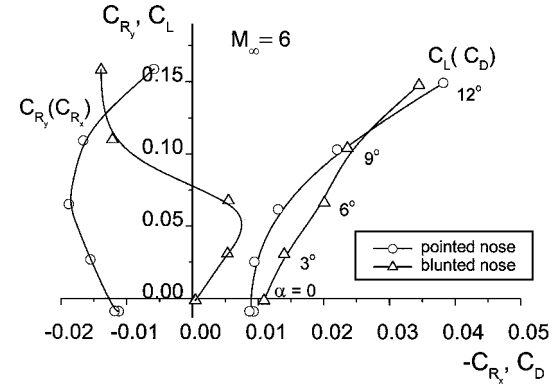

Fig. 16 Polars of aerodynamic forces $C_L(C_D)$ and resultant aeropropulsive forces $C_{R_y}(C_{R_x})$ for $M_\infty = 6$; model variants with blunted and pointed nose tips.

the maximum of the lift-to-drag ratio for $M_\infty = 6$ for the blunted configuration was reached at significantly greater angles of attack $\alpha_{(L/D)_{\max}} = 10$–11 deg as compared to $\alpha_{(L/D)_{\max}} = 6$–7 deg for the pointed configuration.

It would appear reasonable that the decrease in the flow-rate factor of the inlet and the increase in the drag coefficient caused by nose bluntness will lead to deterioration of the resultant aeropropulsive characteristics of the vehicle. For example, the thrust coefficient C_T calculated for the blunted model configuration, as compared to the pointed variant, is very low within the range of angles of attack $\alpha = 0$–8 deg, with a corresponding significant decrease in the experimental flow-rate factor (see Fig. 15). As a consequence, the engine thrust obtained does not compensate for the elevated drag of the configuration caused by nose bluntness and does not ensure the resultant propulsive tangential force for these angles of attack (Fig. 16). However, a positive tangential force occurs for larger angles of attack $\alpha > 6$ deg. An extraordinary S-shaped resultant-force polar for the blunted model configuration is obtained. One would expect some special instability properties, which would be reflected by the said extraordinary S-shaped resultant-force polar, for a vehicle configuration with a blunted nose of the lifting body. For $M_\infty = 4$, the changes in aerodynamic and resultant aeropropulsive characteristics caused by nose bluntness are the same in the qualitative sense but are less significant in magnitude.

The noted extraordinary behavior of the resultant aeropropulsive forces, by the data obtained, is a consequence of unusual varying of the inlet flow rate. Because of scanty measurement on inlet flow patterns, one could only conjecture from general considerations that this peculiarity is a summed effect of realignment of flow around the blunted forebody in comparison to the pointed one, including both the inviscid flow and the boundary layer or a more extended viscid flow near its surface. All of these effects invite a more detailed investigation.

Conclusions

Some factors of inlet/airplane interaction were experimentally studied for a hypersonic scramjet-powered vehicle with a ventral position of the engine nacelle. Experimental aerodynamic characteristics are supplemented by calculated estimates of the engine thrust. Thus, the effects of the considered factors on the total aeropropulsive characteristics of the vehicle are determined. The results obtained allow us to make the following conclusions.

1) Diversion of the boundary layer developing ahead of the inlet, with the use of diverter wedges, improves the flow-rate characteristics of the inlet and increases the engine thrust at high flight Mach numbers. Despite the increase in the drag force in this case, an increase in the resultant propulsive force of the vehicle as a whole can be reached with a certain height of the diverter wedges.

2) The arrangement of the side cheeks restricting lateral spillage of flow over the compression wedge ramp of the inlet leads to rather small increments in the flow-rate factor both for Mach numbers $M_\infty < M_d$ and $M_\infty \approx M_d = 6$. This may be explained by effects of

three dimensionality of the flow around the inlet integrated with the forebody, which violate the design flow regime for the inlet itself. For freestream flow conditions with $M_\infty \approx M_d$, the inlet with the side cheeks ensures a lower drag of the model as compared to the noncheeked inlet variant. Correspondingly, the resultant propulsive force of the vehicle increases in the first case. For $M_\infty = 4 < M_d$, by contrast, the noncheeked inlet provides lower drag, therewith there is a minor effect of increasing of the resultant propulsive force of the vehicle.

3) Nose bluntness of the lifting body is responsible for development of a thick near-wall viscous-entropy layer on the forebody precompression surface, especially for small angles of attack. This leads to an increase in the vehicle drag and to significant losses in the flow-rate factor and engine thrust at near-zero angles of attack, and, as a consequence, the resultant aeropropulsive characteristics of the vehicle as a whole become much worse.

The approach used in the presented study on the problem of inlet/airplane interaction is based on experiments and calculations. An important merit of such an approach is its comprehensiveness and the possibility to consider flight properties of the vehicle as a whole, including the airplane and the engine. At the same time, in this study, the extrapolation of the experimental aerodynamic characteristics to a full-scale vehicle and determination of the engine thrust are rather simplified. The inlet is not fully represented, the parameters of its internal section downstream of the entrance are assumed, and the engine thrust is determined on the basis of a one-dimensional scramjet model. This does not allow one to consider in detail operability issues and performance quantities of the engine, such as inlet starting, engine flow stability, distortion, fueling, effects of engine cross-sectional areas, etc. That is why the results presented are not absolute, but they give a general idea about possible aeropropulsive properties of the vehicle under consideration, which call for further investigation.

References

[1]Starukhin, V. P., and Taryshkin, A. G., "Investigation of Parameters of the Boundary Layer Upstream of the Entrance of a Supersonic Two-Dimensional Inlet Mounted Under the Plane Surface of a Delta Wing," *Uchjonye Zapiski TsAGI (Scientific Notes of Central AeroGydrodynamic Institute)*, Moscow, Vol. 13, No. 2, 1982, pp. 69–77 (in Russian).

[2]Bosnyakov, S. M., Starukhin, V. P., and Chevagin, A. F., "Effect of a Delta Wing on Characteristics of a Two-Dimensional Inlet Mounted Under the Wing," *Uchjonye Zapiski TsAGI (Scientific Notes of Central AeroGydrodynamic Institute)*, Moscow, Vol. 25, No. 1–2, 1994, pp. 67–75 (in Russian).

[3]Goldfeld, M. A., Lisenkov, I. G., and Shcherbik, D. V., "Experimental Study of Three-Dimensional Boundary Layer on a Supersonic Aircraft Surface," *Proceedings of International Conference on the Methods of Aerophysical Research*, Inst. of Theoretical and Applied Mechanics, Russian Academy of Sciences Press, Siberian Branch, Novosibirsk, Pt. 2, 1994, pp. 96–101.

[4]Lawing, P. L., and Johnson, C. B., "Inlet Boundary-Layer Shapes on Four Aircraft Forebodies at Mach 6," *Journal of Aircraft*, Vol. 15, No. 1, 1978, pp. 62, 63.

[5]Johnson, C. B., and Lawing, P. L., "Mach 6 Flowfield Survey at the Engine Inlet of a Research Airplane," *Journal of Aircraft*, Vol. 14, No. 4, 1977, pp. 412–414.

[6]Vasil'ev, V. I., "Problems of Designing Inlets for Supersonic Passenger Aircraft," *Trudy TsAGI (Transactions of Central AeroGydrodynamic Institute)*, No. 1501, 1973, pp.1–18 (in Russian).

[7]Zheltovodov, A. A., Rafaelyants, A. A., and Filatov, V. M., "Investigation of Drag and Special Features of Flows Around Wedges for Boundary Layer Diversion," *Aerodynamic Interference in the Flows Around Three-Dimensional Bodies*, Inst. of Theoretical and Applied Mechanics, Academy of Sciences of the USSR Press, Siberian Branch, Novosibirsk, 1980, pp. 63–82 (in Russian).

[8]Goonko, Y. P., Mazhul, I. I., and Shcherbik, D. V., "Effect of Boundary-Layer Bleeding on the Aeropropulsive Efficiency of a Hypersonic Vehicle," *Izvestiya VUZ'ov, Aviatsionnaya Tekhnika (News of Institutions of Higher Education, Aviation Technology Series)*, No. 1, 1993, pp. 89–92 (in Russian).

[9]Goonko, Y. P., Mazhul, I. I., and Shcherbik, D. V., "Effect of Boundary-Layer Bleeding on Performance of an Inlet and the Hypersonic Scramjet-Powered Vehicle as a Whole," *Thermophysics and Aeromechanics*, Vol. 7, No. 2, 2000, pp. 173–185.

[10]Bosnyakov, S. M., and Remeev, N. K., "Investigation of Three-Dimensional Supersonic Flow Around a Two-Dimensional Inlet with Side Cheeks," *Uchjonye Zapiski TsAGI (Scientific Notes of Central AeroGydrodynamic Institute)*, Vol. 11, No. 5, 1980, pp. 40–45 (in Russian).

[11]Bosnyakov, S. M., Bykova, S. A., and Remeev, N. K., "Investigation of Three-Dimensional Flow and Aerodynamic Characteristics of Two-Dimensional Inlets with Different Entrance Shape and Size of Side Cheeks," *Uchjonye Zapiski TsAGI (Scientific Notes of Central AeroGydrodynamic Institute)*, Vol. 14, No. 3, 1983, pp. 107–113 (in Russian).

[12]Vinogradov, V. A., Duganov, V. V., Zakharov, N. N., Ivanov, M. Y., and Ivanov, O. K., "Experimental and Numerical Studies of Supersonic Flow over the Wedge Ramp of a Two-Dimensional Inlet," TR of CIAM (Central Inst. of Aviation Motor Building), CIAM TR 8198, Moscow, 1977, pp. 1–69 (in Russian).

[13]Starukhin, V. P., and Chevagin, A. F., "Effect of Bluntness of Entrance Edges on Characteristics of Inlets Mounted Under a Wing," *Uchjonye Zapiski TsAGI (Scientific Notes of Central AeroGydrodynamic Institute)*, Vol. 25, No. 1–2, 1994, pp. 89–100 (in Russian).

[14]Bakharev, S. A., Gurylev, V. G., and Kosykh, A. P., "Aerodynamic Characteristics of a Blunted Delta Wing with Simulation of Air Flow Through an Inlet at Supersonic and Hypersonic Velocities," *Uchjonye Zapiski TsAGI (Scientific Notes of Central AeroGydrodynamic Institute)*, Pt. 2, Vol. 22, No. 1, 1991, pp. 39–47 (in Russian).

[15]Aleksandrovich, E. V., "Drag of Blunted Edges of Supersonic and Hypersonic Inlets," *Tekhnika Vozdyshnogo Flota (Airfleet Machinery—Journal of Aviation Science and Technology)*, No. 6, 1997, pp. 9–18 (in Russian).

[16]Goonko, Y. P., "Aerodynamic Experimentation with Ducted Models as Applied to Hypersonic Air-Breathing Vehicles," *Experiments in Fluids*, Vol. 27, No. 3, 1999, pp. 219–234.

[17]Volonikhin, I. I., Grigor'ev, V. D., Dem'janenko, V. S., Pisarenko, K. I., and Kharitonov, A. M., "Supersonic Wind Tunnel T-313," *Aerophysical Research,* Inst. of Theoretical and Applied Mechanics, Academy of Sciences of the USSR Press, Siberian Branch, Novosibirsk, 1972, pp. 8–11 (in Russian).

[18]Goonko, Y. P., "Experimental Comparison of Aerometric Techniques for Determination of the Total Flow-Rate of Supersonic Non-Uniform Streams," Preprint, Inst. of Theoretical and Applied Mechanics, Academy of Sciences of the USSR, Siberian Branch, Novosibirsk, No. 2, 1981, pp. 1–27 (in Russian).

[19]Blisch, V. G., "External and Internal Aerodynamic Forces and Moments Acting on Air-Breathing Vehicles and Their Models at Non-Zero Angles of Attacks," *Trudy TsAGI (Transactions of Central AeroGydrodynamical Institute)*, No. 2328, 1987, pp. 1–17 (in Russian).

[20]Mazhul, I. I., "Some Peculiarities of Approximate Calculation of Aerodynamic Characteristics for Polyhedral Lifting Bodies at Supersonic Flight Velocities," *Izvestiya SO AN SSSR, Seriya Tekhnicheskikh Nauk (News of Siberian Branch of Academy of Sciences of the USSR, Series of Technical Sciences)*, No. 16, 1986, pp. 52–57 (in Russian).

[21]Briggs, J. L., "Comment on Calculation of Oblique Shock Waves," *AIAA Journal*, Vol. 2, No. 5, 1964, p. 974.

[22]Hui, W. H., "Simple Formulae for Supersonic Flow Past a Cone," *Aeronautical Quarterly*, Vol. 26, Pt. 1, 1975, pp. 11–19.

[23]Beloglazkin, A. N., Goonko, Y. P., Koshcheev, A. B., and Mazhul, I. I., "Calculation and Analysis of Aerodynamic and Total Aero-Propulsive Characteristics of a Scramjet-Powered Hypersonic Vehicle," *Aerothermodynamics of Aerospace Systems, Proceedings of Annual TsAGI Workshop "Fluid and Gas Mechanics,"* TsAGI (Central AeroGydrodynamic Inst.), Moscow, 1992, pp. 51–60 (in Russian).

[24]Goonko, Y. P., and Mazhul, I. I., "Estimations on Integral Aerogasdynamics of Hypersonic Scramjet-Powered Aircraft," *Thermophysics and Aeromechanics*, Vol. 2, No. 3, 1995, pp. 203–213.

[25]Swithenbank, J., "Hypersonic Air-Breathing Propulsion," *Progress in Aeronautical Sciences*, Vol. 8, Pergamon, Oxford, England, U.K., 1967, pp. 229–296.

[26]Zuev, V. S., and Makaron, V. S., "Theory of Ramjet and Rocket-Ramjet Engines," Mashinostroenie (Mechanical Engineering), Moscow, 1971, pp. 1–367 (in Russian).

[27]Hasinger, S. H., "A New Method for Calculating Ducted Flows," *AIAA Journal*, Vol. 22, No. 1, 1984, pp. 141–143.

[28]Armangaud, F., Decher, R., and Koopman, A., "One-Dimensional Modeling of Hypersonic Flight Propulsion Engines," AIAA Paper 89-2026, 1989.

[29]Struminsky, V. V., Kharitonov, A. M., and Chernykh, V. V, "Experimental Study on Transition of Laminar Boundary Layer to Turbulent One at Supersonic Velocities," *Mechanika Zhidkosti i Gasa (Journal of Fluid and Gas Mechanics)*, No. 2, 1972, pp. 30–34 (in Russian).

[30]Kalinina, S. V., and Kornilov, V. I., "Effects of Sweep Angle and Unit Reynolds Number on Boundary-Layer Transition at Supersonic Velocities," *Prikladnaya Matematika i Tekhnicheskaya Physika (Journal of Applied Mathematics and Technical Physics)*, No. 1, 1973, pp. 159–162 (in Russian).

[31]Kovalenko, V. M., "Calculation of Friction and Heat Transfer Coefficients for a Flat Plate in the Presence of Heat Transfer at Supersonic Speeds," *Transactions of Central Aerogydrodynamic Institute (TsAGI)*, No. 1084, 1967, pp. 1–51 (in Russian).

[32]Spalding, D. B., and Chi, S. W., "The Drag of a Compressible Turbulent Boundary Layer on a Smooth Flat Plate with and Without Heat Transfer," *Journal of Fluid Mechanics,* Vol. 18, Pt. 1, 1964, pp. 117–143.

[33]Goonko, Y. P., Kudryavtsev, A. N., Mazhul, I. I., and Rakhimov, R. D., "Some Comparison of Flows Around Hypersonic Aircraft Whose Forebodies are Integrated with Two-Dimensional and Three-Dimensional Convergent Inlets," *Proceedings of International Conference on the Methods of Aerophysical Research (ICMAR-2000)*, Russian Academy of Sciences Press, Siberian Branch, Novosibirsk, Pt. 1, 2000, pp. 104–109.